JCI insight

Exogenous sickle erythrocytes combined with vascular disruption trigger disseminated tumor vaso-occlusion and lung tumor regression

Chiao-Wang Sun, … , Tim M. Townes, David S. Terman

JCI Insight. 2019;4(7):e125535. https://doi.org/10.1172/jci.insight.125535.

Research Article **Hematology** **Oncology**

Hypoxic tumor niches are chief causes of treatment resistance and tumor recurrence. Sickle erythrocytes' (SSRBCs') intrinsic oxygen-sensing functionality empowers them to access such hypoxic niches wherein they form microaggregates that induce focal vessel closure. In search of measures to augment the scale of SSRBC-mediated tumor vaso-occlusion, we turned to the vascular disrupting agent, combretastatin A-4 (CA-4). CA-4 induces selective tumor endothelial injury, blood stasis, and hypoxia but fails to eliminate peripheral tumor foci. In this article, we show that introducing deoxygenated SSRBCs into tumor microvessels treated with CA-4 and sublethal radiation (SR) produces a massive surge of tumor vaso-occlusion and broadly propagated tumor infarctions that engulfs treatment-resistant hypoxic niches and eradicates established lung tumors. Tumor regression was histologically corroborated by significant treatment effect. Treated tumors displayed disseminated microvessels occluded by tightly packed SSRBCs along with widely distributed pimidazole-positive hypoxic tumor cells. Humanized HbS-knockin mice (SSKI) but not HbA-knockin mice (AAKI) showed a similar treatment response underscoring SSRBCs as the paramount tumoricidal effectors. Thus, CA-4-SR–remodeled tumor vessels license SSRBCs to produce an unprecedented surge of tumor vaso-occlusion and infarction that envelops treatment-resistant tumor niches resulting in complete tumor regression. Strategically deployed, these innovative tools constitute a major conceptual advance with compelling translational potential.

JCI insight

RESEARCH ARTICLE

Exogenous sickle erythrocytes combined with vascular disruption trigger disseminated tumor vaso-occlusion and lung tumor regression

Chiao-Wang Sun,[1] Li-Chen Wu,[1] Mamta Wankhede,[2] Dezhi Wang,[3] Jutta Thoerner,[4] Lawrence Woody,[4] Brian S. Sorg,[5] Tim M. Townes,[1] and David S. Terman[1]

[1]Department of Biochemistry and Molecular Genetics, University of Alabama School of Medicine at Birmingham, Birmingham, Alabama, USA. [2]Department of Biomedical Engineering, University of Pittsburgh School of Medicine, Pittsburgh, Pennsylvania, USA. [3]Department of Pathology, University of Alabama School of Medicine at Birmingham, Birmingham, Alabama, USA. [4]Histopathology Section, Hospital of the Monterey Peninsula, Monterey, California, USA. [5]Cancer Diagnosis Program, National Cancer Institute, Bethesda, Maryland, USA.

Hypoxic tumor niches are chief causes of treatment resistance and tumor recurrence. Sickle erythrocytes' (SSRBCs') intrinsic oxygen-sensing functionality empowers them to access such hypoxic niches wherein they form microaggregates that induce focal vessel closure. In search of measures to augment the scale of SSRBC-mediated tumor vaso-occlusion, we turned to the vascular disrupting agent, combretastatin A-4 (CA-4). CA-4 induces selective tumor endothelial injury, blood stasis, and hypoxia but fails to eliminate peripheral tumor foci. In this article, we show that introducing deoxygenated SSRBCs into tumor microvessels treated with CA-4 and sublethal radiation (SR) produces a massive surge of tumor vaso-occlusion and broadly propagated tumor infarctions that engulfs treatment-resistant hypoxic niches and eradicates established lung tumors. Tumor regression was histologically corroborated by significant treatment effect. Treated tumors displayed disseminated microvessels occluded by tightly packed SSRBCs along with widely distributed pimidazole-positive hypoxic tumor cells. Humanized HbS-knockin mice (SSKI) but not HbA-knockin mice (AAKI) showed a similar treatment response underscoring SSRBCs as the paramount tumoricidal effectors. Thus, CA-4-SR–remodeled tumor vessels license SSRBCs to produce an unprecedented surge of tumor vaso-occlusion and infarction that envelops treatment-resistant tumor niches resulting in complete tumor regression. Strategically deployed, these innovative tools constitute a major conceptual advance with compelling translational potential.

Introduction

Hypoxic tumor niches and their underlying molecular axes have been a chief target of molecular cancer therapeutics. Of paramount concern to investigators is that such niches are associated with resistance to conventional cancer treatment, and their persistence is a major cause of tumor recurrence (1–3). Under hypoxic conditions within tumors, conserved oxygen sensors activate hypoxia-inducible transcription factors and proangiogenic signals (4). The latter induce a disordered network of blood vessels resulting in cyclic or chronic deoxygenation (5). As tumor growth outscales neoangiogenesis, tumor cells rendered chronically hypoxic may survive, proliferate, and become treatment resistant (6).

The failure of conventional treatment has prompted a universal search for conceptually new tools and strategies to eradicate these treatment-resistant hypoxic tumor cell subpopulations. Antiangiogenic agents that limit the tumor blood supply to these niches by targeting receptors on embryonic blood vessels usually lead to tumor regrowth by activating alternate synthetic pathways, hypoxia-inducible factors, or tumor cells that evade the effect of therapy (7–9). Likewise, polymeric nanocarriers occlude only a fraction of mature tumor blood vessels and in the absence of hypoxia-sensing systems fail to access oxygen-deprived regions (10, 11). We therefore turned to the SSRBCs derived from a mutated erythroid lineage. These cells circulate freely and possess a unique hypoxia-sensing functionality, which becomes operative under severely hypox-

Conflict of interest: The authors have declared that no conflict of interest exists.

Submitted: October 12, 2018
Accepted: February 14, 2019
Published: April 4, 2019.

Reference information: *JCI Insight*. 2019;4(7):e125535. https://doi.org/10.1172/jci.insight.125535.

ic conditions in low-velocity microvessels (12, 13). SSRBCs are trapped in these vessels leading to HbS desaturation, polymerization, and formation of tetrameric spicules rendering them rigid, adhesive, and prone to vaso-occlusive aggregation (12, 14). Intravital microscopy observations show that infused SSRBCs home to established tumor, form aggregates in tumor vessels, and induce focal vessel closure. Together with pro-oxidants or oncogenic virus, SSRBCs also induce a therapeutic tumor growth delay but fail to produce complete tumor regressions (15, 16).

In search of agents that could increase the efficiency and scale of SSRBC-mediated tumor killing, we turned to the vascular disrupting agent, combretastatin A4 (CA-4). The latter is derived from the South African bushwillow tree, *Combretum caffrum*. It binds to tumor endothelial β-tubulin subunits, inhibits microtubule formation, and induces cytoskeletal alterations leading to vascular collapse, blood stasis, focal hypoxia, and ischemic tumor cell necrosis (17–19). Despite these potent effects, CA-4 and its diphosphate derivative fail to eliminate viable tumor cells at the tumor rim, resulting in rapid tumor regrowth (20, 21). Combining CA-4 with other therapeutics such as radiation, cytotoxics, antiangiogenics, and biologics failed to alleviate the peripheral tumor regrowth in murine tumor models (17, 22–24).

We hypothesized that CA-4's selective induction of tumor endothelial cell injury, blood stagnation, and hypoxia could create a microvascular milieu wherein SSRBCs could efficiently deoxygenate, form microaggregates, and induce a broad scale of tumor vessel closure and infarction. Such massive vaso-occlusion infarction could not only encompass hypoxic niches but also the treatment-resistant tumor rim. To this end, we introduce hypoxia-reactive SSRBCs as a biotherapeutic whose physiologic adaptation to CA-4–induced tumor blood stasis and microvascular hypoxia results in an unprecedented scale of tumor microvessel closure and infarction that obliterates treatment-resistant hypoxic niches and the tumor rim. The SSRBC–CA-4 regimen produced complete tumor regressions, whereas each therapeutic alone or combined with conventional antiangiogenics, cytotoxics, or radiation resulted in tumor progression. Collectively, these findings provide conceptually new tools, mechanisms, and strategies whereby drug-induced tumor endothelial remodeling licenses broad propagation of SSRBC-mediated vessel closure culminating in tumor eradication.

Results

Assessment of vascular disrupting agent ability to induce hypoxia in Caki-1 and Lewis lung carcinoma. Using hyperspectral imaging, we assessed the spatial and kinetic effects of CA-4 on the development and recovery of tumor hypoxia, vascular collapse, and parenchymal injury in the Caki-1 tumor. In Figure 1, representative of 2 experiments, hyperspectral imaging of the untreated Caki-1 tumor displayed an area of 38% with an hemoglobin (Hb) saturation of less than 10% (Figure 1, A, D, and G). Four hours after treatment with CA-4, 63% of the tumor area exhibited less than 10% Hb saturation, while light-field microscopy showed collapse of tumor microvessels at the tumor core ($P \leq 0.000002$, Figure 1, B, E, and G). At 48 hours, bright-field observations revealed obliteration of tumor vessels in the tumor core, while hyperspectral imaging showed partial recovery of oxygenation in the tumor periphery (Figure 1, C, F, and G). Although these observations are consistent with previous reports (25, 26), we postulated that tumor microvascular hypoxia (Hb sat < 10%) and vessel collapse of this order induced by CA-4 within 4 hours after administration would enable SSRBCs to deoxygenate and their HbS to polymerize as shown in vitro by Noguchi et al. (27). Under these conditions, SSRBCs also assume the sickle morphology and upregulate intrinsic adhesion receptors resulting in SSRBC aggregation and vaso-occlusion. The narrow time dependency for induction of tumor vascular hypoxia and vessel and collapse by these agents indicated that to optimize the vaso-occlusive effect of SSRBCs, both SSRBCs and CA-4 would need to be administered at the same time. Because of their biocompatibility with humanized HbS-knockin mice (SSKI) mice, we carried out additional studies of tumor hypoxia with CA-4 alone and combined with SSRBCs and SR as discussed (below) using the venerable pimidazole hypoxia marker in C57BL/6J mice bearing established Lewis lung carcinoma (LLC) (Figure 2, A–C). Intracellular pimidazole is activated in vivo by deoxygenation in a range of 0%–10% mmHg similar to that noted after CA-4 administration to the Caki-1 tumors (28).

Transfused sickle cells induce a vaso-occlusive surge in response to CA-4 and SR resulting in broadly propagated tumor hypoxia and infarction engulfing the core and treatment-resistant tumor rim. Next, we determined whether SSRBCs transfused together with CA-4 could induce vaso-occlusion and hypoxia in the microvessels of established LLC. We selected the LLC in C57BL/6J mice for its biocompatibility with SSKI mice whose SSRBCs would be used for the transfusion. These strains share a common background and reject the LLC in a similar fashion. Mice with established LLC were treated with CA-4, alone or together with infusion of SSRBCs obtained from SSKI mice and sacrificed 24 hours later. Tumor section analysis showed a modest

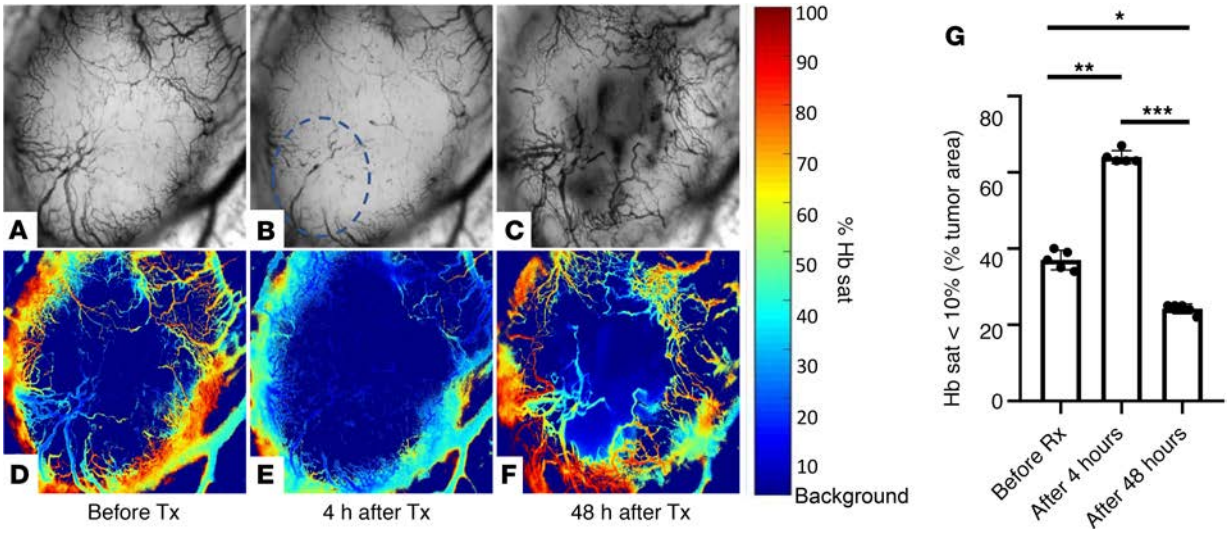

Figure 1. Brightfield and corresponding hemoglobin saturation images of an established Caki-1 tumor before and after CA-4 administration. (**A**, **D**, and **G**) Pretreatment images show original vascular structure with Hb saturation of less than 10% enveloping 38% of the tumor area. (**B**, **E**, and **G**) Four hours after CA-4 administration, tumor vessels in the tumor exhibit vascular collapse (circle, compare **B** and **A**) associated with Hb saturation of less than 10% covering 64% of the tumor area. $^{**}P \leq 0.000002$ compared with pretreatment values. (**C** and **F**) Forty-eight hours after CA-4 administration, core vessels show oxygenation recovery with Hb saturation less than 10% engulfing 24% of the tumor surface. $^{*}P \leq 0.00005$ and $^{***}P \leq 0.000001$ compared with pretreatment and 4-hour posttreatment levels respectively, by 2-tailed Student's *t* test. Images were obtained at ×2.5 original magnification with image dimensions of 4.15 × 3.125 mm. The color scale shows percentage Hb saturation values. $n = 5$ separate readings of Hb saturation less than 10% using ImageJ software to determine percentage tumor area.

degree of vaso-occlusion and pimidazole-reactive hypoxic cells in the treated groups (Figure 2C). We next examined the effect of SR to the tumor alone or together with CA-4 or SSRBCs on tumor vaso-occlusion and hypoxia. We reasoned that because tumor SR induces mitotically based reactive oxygen species–driven (ROS) tumor endothelial apoptosis and it could augment the vascular injury, tumor hypoxia and vaso-occlusion induced by CA-4 and SSRBCs (29–31). After adding tumor SR to CA-4, we observed a significant increase in pimidazole-reactive tumor cells encompassing 40% of the tumor area (Figure 2C). We therefore combined tumor SR and CA-4 with SSRBC infusions. Mice with established tumors were treated with SR to the tumor and 24 hours later received CA-4 with infusion of SSRBCs. Surprisingly, tumor sections obtained 24 hours after concluding treatment showed massive tumor microvessel closure and associated infarction that engulfed the core and the treatment-resistant tumor rim (Figure 3, A–E). Simultaneously, the SSRBC-based triple therapy significantly increased the tumor hypoxic fraction and limited the number of proliferating Ki-67^{+} tumor cells (Figure 2C and Figure 4, A–C). Mice similarly treated with HbA-RBCs (AARBCs) obtained from humanized HbA-knockin mice (AAKI mice) showed a significantly lower degree of tumor vaso-occlusion, hypoxia, and infarction than SSKI mice; mice treated with single or dual modalities showed minimal vaso-occlusion, infarction, and hypoxia (Figure 2D and Figure 3E). These results indicate that SSRBCs work synergistically with CA-4 and tumor SR to broadly propagate tumor vaso-occlusion, hypoxia, and infarction. Importantly, the massive infarctions induced by SSRBC-based triple therapy obliterated pimidazole-positive pockets and the treatment-resistant tumor rim (Figure 2C and Figure 3, A–E). CA-4 and tumor SR were more effective in inducing tumor hypoxia (Figure 2C) than either one alone, suggesting that cumulative tumor microvessel conditioning/injury induced by these modalities unleashes a robust SSRBC-mediated vaso-occlusive and tumoricidal response.

Repeated sickle cell infusions induce regression of established LLC when combined with CA-4 and SR. Having shown that SSRBC infusions with CA-4 and tumor SR could produce disseminated tumor vaso-occlusion, hypoxia, and infarction encompassing the tumor rim, we next determined whether repeated treatment of established lung tumors with the triple regimen could induce significant tumor regressions. Mice with established LLC were treated with SR to the tumor on day 12 and 24 hours later (day 13) received CA-4 along with infusions of SSRBCs obtained from SSKI mice or humans with sickle cell anemia. SSRBC infusion and CA-4 were repeated on days 15 and 18 and mice were sacrificed on day 22. Results showed that mouse or human SSRBCs coupled with CA-4 and SR produced significant arrest of LLC growth on day 22

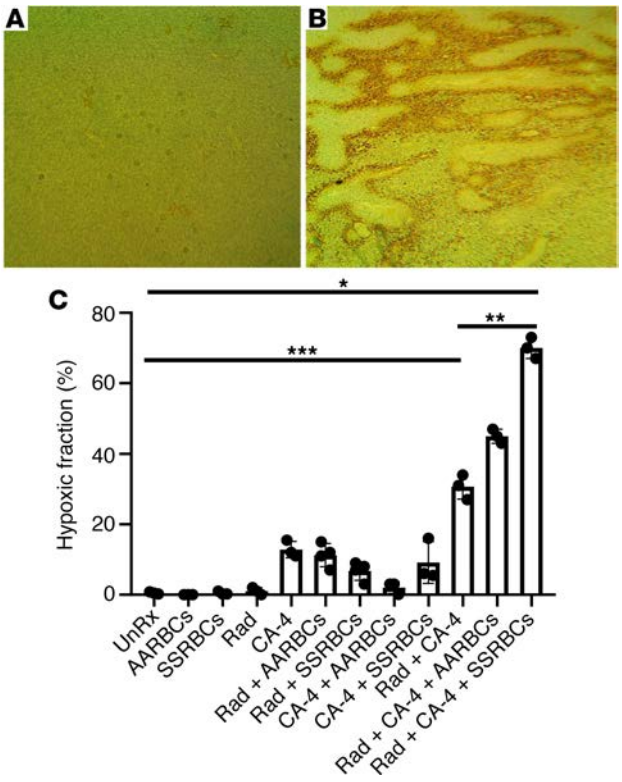

Figure 2. Fractional uptake of pimidazole (hypoxic fraction) in sections of LLC in C57BL/6J mice obtained on day 14 after treatment with tumor SR (10 Gy) to the tumor on day 12 followed by CA-4 plus passive infusion of SSRBCs or AARBCs on day 13. (**A**) Pimidazole uptake in LLC cells in untreated mice and (**B**) in mice treated with SSRBC-based triple therapy is shown. (**C**) Hypoxic fraction in tumor sections after treatment with SSRBC-based triple therapy exceeded that of AARBC-based triple therapy and the combination of sublethal radiation plus CA-4 treatment (***$P \leq 0.0009$). Hypoxic fraction of radiation plus CA-4 combined exceeded that of all other dual or single treatments (**$P \leq 0.001$). Hypoxic fraction in mice treated with SSRBC-based triple therapy also exceeded that of mice receiving all other treatments. *$P \leq 0.0001$ by 2-tailed Student's *t* test (n = 3). Diaminobenzidine (DAB, Scy Tek Laboratories) was used as the chromagen. The area showing pimidazole staining was determined using ImageJ software and the analyses performed at ×10 original magnification. Fractional area of pimidazole positivity was computed as a percentage of the total tumor area. Fraction of immunohistochemically hypoxic cells (IHFs) was calculated as: IHF = AF_{pim}/A_{total} in which AF_{pim} is the fraction showing pimonidazole staining and A_{total} is the total tumor area.

(Figure 5A). By contrast, mice similarly treated with red blood cells (RBCs) from AAKI mice or a normal human donor showed tumor progression (Figure 5A). Combining SSRBC infusions with CA-4 or tumor SR individually or administering CA-4 together with tumor SR without SSRBC infusions produced LLC progression (Figure 5A). Analysis of tumor sections from mice passively infused with mouse or human SSRBCs plus CA-4 and SR on day 22 showed extensive tumor vaso-occlusion and infarction enveloping the core and tumor periphery (Figure 5, B and C). In the SSRBC-based triple therapy group, residual viable tumor area was confined to less than 5% of the tumor area, providing histologic corroboration for the observed tumor regressions (Figure 6). This reduction in residual viable tumor area was significantly lower than in mice similarly treated with mouse or human AARBCs and controls receiving single or dual agents (Figure 6). Collectively, these data demonstrate the ability of passively infused SSRBCs to induce tumor regressions in vivo when combined with CA-4 and tumor SR. They further underscore the primacy of SSRBCs over AARBCs in the tumoricidal process.

SSKI but not AAKI mice treated with CA-4 and SR exhibit tumor regressions affirming the primacy of SSRBCs in the tumoricidal response in vivo. Having shown that passive infusions of SSRBCs but not AARBCs induced tumor regression in mice in combination with CA-4 and tumor SR, we hypothesized that repeated treatment of SSKI but not AAKI mice would recapitulate the tumoricidal response. SSKI or AAKI mice with established lung tumors were treated with SR on day 12 followed by CA-4 on days 13, 15, and 18. Treatment with tumor SR or CA-4 individually failed to retard LLC growth (Figure 7A). By contrast, treatment of SSKI mice but not AAKI mice with tumor SR plus CA-4 three times completely abolished LLC growth (Figure 7A). Analysis of tumor sections from SSKI mice treated with CA-4 and tumor SR showed broadly propagated tumor infarctions engulfing the core and tumor periphery associated with tumor cell necrosis, mononuclear cell infiltration, and a significantly greater number of occluded microvessels as well as a significantly smaller area of residual viable tumor than similarly treated AAKI mice (Figure 7, B–D and Figure 8, A and B). The SSRBC-mediated vessel occlusions were often clustered and tightly packed with erythrocytes of which nearly 100% exhibited a sickle cell morphology (Figure 7C). Because only 5% of circulating nondeformable sickle cells in SSKI mice display the sickle morphology (15), it is likely that SSRBCs trapped in the injured tumor microvessels transitioned to the sickle shape as their HbS deoxygenated and polymerized. That therapy with SR and CA-4 in SSKI but not AAKI mice can induce tumor regression in vivo confirms the key role of SSRBCs in the vaso-oc-

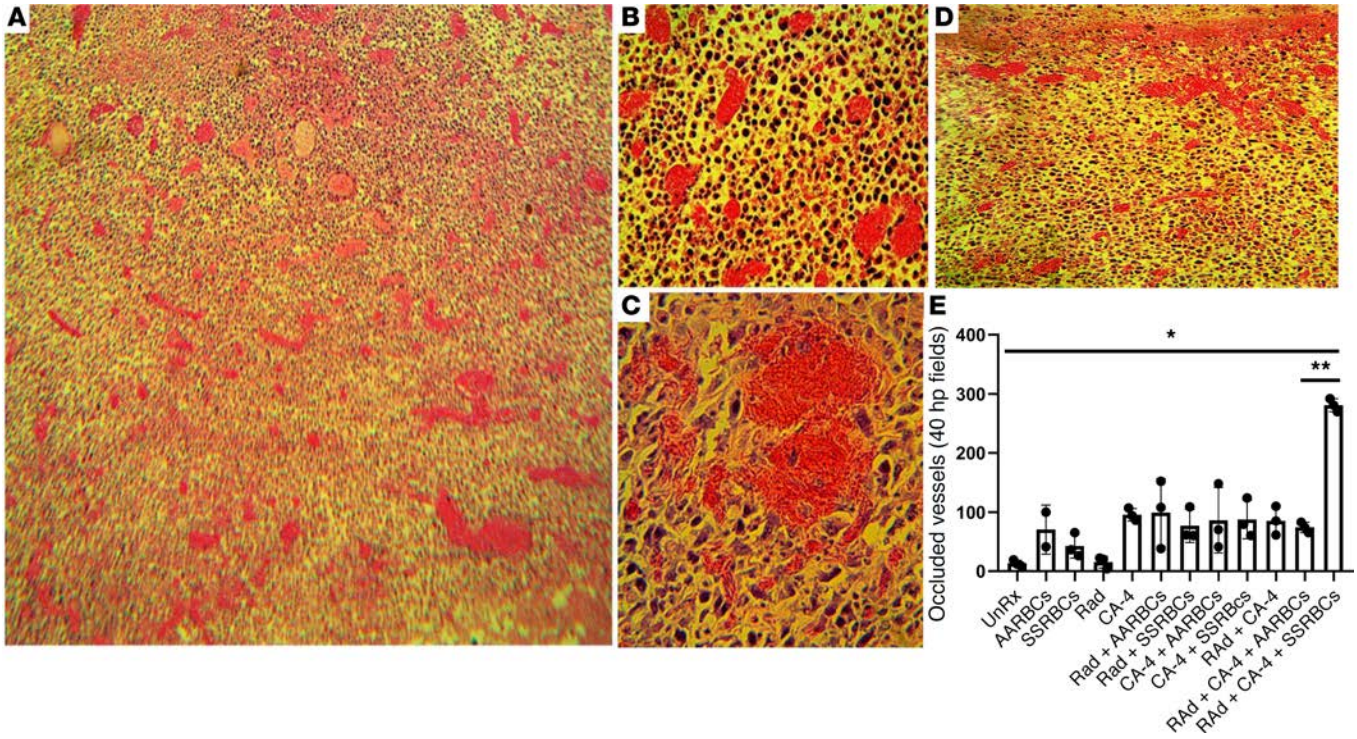

Figure 3. Histopathology and quanfication of vaso-occlusion in sections of LLC in C57BL/6J mice obtained on day 14 after treatment with tumor SR (10 Gy) on day 12 followed by CA-4 plus passive infusion of SSRBC or AARBC on day 13. Tumor sections from mice receiving SSRBC-based triple therapy shows (**A**) disseminated tumor vaso-occlusion, adjacent tumor cell necrosis, and mononuclear cell infiltration (original magnification, ×10); (**B**) clustered tumor vessel occlusions surrounded by mononuclear cells (original magnification, ×25); (**C**) tumor vessels with tightly packed sickle cells (original magnification, ×40). (**D**) Shows extensive vaso-occlusion with mononuclear cell infiltration engulfing the tumor periphery (original magnification, ×25). (**E**) Demonstrates that the number of occluded tumor microvessels after treatment with SSRBC-based triple therapy exceeded that of similar AARBC-based triple therapy (**P = 0.00009) and all dual and single treatments (*$P \leq 0.0001$, 2-tailed Student's t test; $n = 3$). Tumor vaso-occlusion was quantified in tumor sections by enumerating the total number of occluded microvessels in 40 fields at ×40 original magnification. Microvessels were considered occluded when at least 80% of the vessel lumen was filled with erythrocytes.

clusive tumoricidal process. These data show for the first time a powerful synergy between these tools resulting in a sharp surge of tumor vaso-occlusion and infarction, comprehensive in scale that eradicates the core and treatment-resistant tumor rim with consequent tumor regression.

Toxicity of treatments. The treatments were well tolerated at the specified doses. Histologic analysis of heart, lungs, kidneys, and liver of SSKI mice treated with CA-4 and radiation-treated tumor-bearing SSKI mice or similarly treated tumor-bearing C57BL/6J mice passively infused with SSRBCs showed no evident vaso-occlusion, thrombosis, infarction, or hemorrhage. Spleens from treated C57BL/6J mice showed no changes from the untreated mice. These findings are in accord with previous reports (32). Compared with C57BL/6J mice, spleens from untreated SSKI mice were significantly enlarged, and red pulp sinusoids were congested with sickle cells with no evidence of old or acute infarctions. Relative to spleens from untreated SSKI mice, spleens from treated SSKI mice showed slightly more sinusoidal congestion but no evident vaso-occlusion, fresh infarction, or hemorrhage.

Discussion

Here, we introduce hypoxia-reactive SSRBCs as a new therapeutic that unleashes massive tumor vaso-occlusion and infarction in the presence of tumor endothelial injury and hypoxia induced by CA-4 and SR. The dynamic chain of events culminates in comprehensive eradication of established tumors engulfing treatment-resistant hypoxic niches and the tumor rim. The treatment effect was selective for tumors and correlated with a major pathological response predictive of prolonged survival in patients with lung cancer (33, 34). SSRBCs were requisite for the tumoricidal response because the antitumor effect occurred in humanized SSKI mice but not in similarly treated AAKI mice. SSRBCs therefore emerge as an indispensable and paramount effector in the profound tumoricidal synergy with CA-4 and SR.

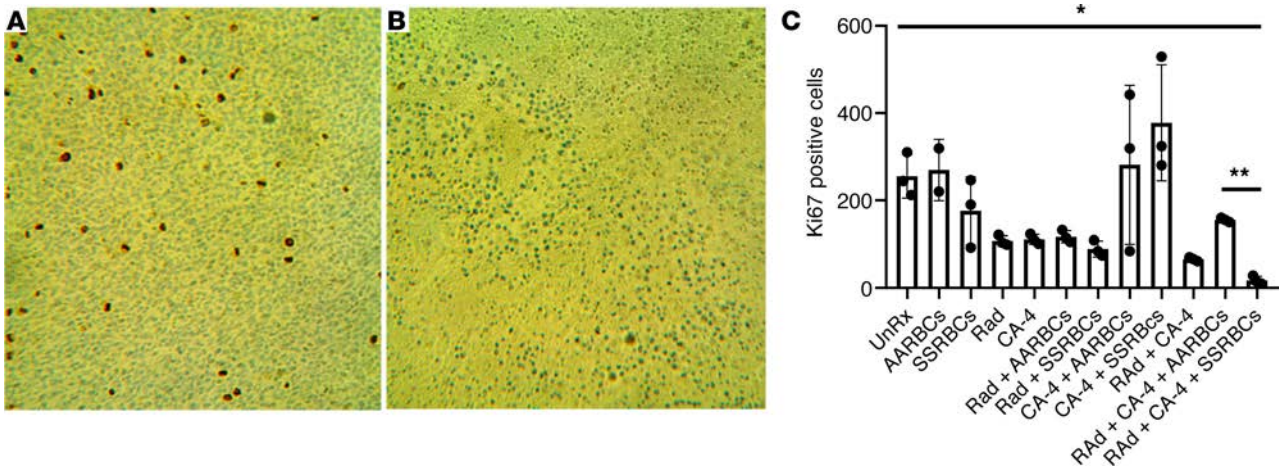

Figure 4. Ki-67 uptake in sections of LLC in C57BL/6J mice obtained on day 14 after treatment with tumor SR (10 Gy) on day 12 followed by CA-4 plus passive infusion of SSRBC or AARBC on day 13. (**A**) Nuclear Ki-67 uptake by LLC cells, an indicator of mitotically active tumor cells, from untreated mice and (**B**) in mice treated with SSRBC-based triple therapy is shown. (**C**) Ki-67 uptake in tumor sections after 1 cycle of SSRBC-based triple therapy was diminished relative to that of AARBC-based triple therapy (**$P \leq 0.0001$, 2-tailed Student's *t* test) and all dual and single treatments (*$P \leq 0.0001$, $n = 3$). Ki-67–immunopositive cells were quantified in tumor sections in 30 separate fields at ×40 original magnification.

As the central therapeutic in the tumoricidal effect, the SSRBC produces broadly propagated tumor vaso-occlusion infarction in the tumor microvasculature conditioned by CA-4-SR–induced hypoxia and vascular injury. In the proposed chain of events (Figure 9), both SR and CA-4 induce endothelial injury, the former via single- and double-stranded DNA breaks and the latter by means of endothelial cytoskeletal/microtubule injury following disruption of the VE-cadherin/β-catenin/Akt signaling pathway (35, 36). The resulting endothelial blebbing and rounding up impinges on the microvascular lumen leading to blood stagnation and the observed significant increase in tumor hypoxia (18, 37). In the face of this profound degree of blood stasis and tumor hypoxia, SSRBC HbS deoxygenates and polymerizes, resulting in increased SSRBC rigidity and blood viscosity. Desaturated SSRBCs trapped in this milieu adhere to vessel walls and form microvascular aggregates to account for broadly propagated vaso-occlusion and the observed appearance of tightly packed SSRBCs in the occluded tumor vessels. Because only 5% of circulating SSRBCs exhibit the sickle morphology, the appearance of sickle-shaped cells in the occluded vessel confirms the key role of drug-induced blood stagnation and hypoxia in the sickle cell transformative process. The disseminated tumor vessel closure explains the observed surge of pimidazole-positive hypoxic tumor cells and extensive infarction in the tumor parenchyma. The widespread tumor cell death is primarily due to infarction-based oxygen deprivation evidenced by the disseminated hypoxia, infarction, mononuclear cell infiltration, sharp reduction in residual viable tumor cells and mitotically active Ki-67–positive cells. Collectively, these finding unveil what we believe is a previously unrecognized synergy between SSRBCs and CA-4-SR, wherein CA-4-SR–induced severe tumor endothelial cell injury unleashes a massive adaptative surge of SSRBC remodeling and tumor vaso-occlusion. The resulting extensive tumor infarctions encompass treatment-resistant hypoxic niches and tumor rim leading to regressions in vivo.

In addition to SSRBCs' unique oxygen sensing functionality and proclivity to autoaggregate, their pro-oxidative membranes and intrinsic heme can also induce ROS-mediated endothelial cell injury (15, 38–40). In the absence of such properties, inert microparticles and micelles used clinically to induce tumor vessel closure produce no more than 30%–60% tumor vaso-occlusion, require locoregional access for administration, and rarely generate complete tumor regression (10, 41). By contrast, the SSRBC-based regimen shown here administered by noninvasive routes induced comprehensive vaso-occlusion and complete tumor regressions. The scale of the observed tumor cell and stromal eradication likely precludes the emergence of intrinsic growth-promoting hypoxia-inducible factors and alternate angiogenic pathways that have hampered the efficacy of antiangiogenics (9, 10). The synergistic tumoricidal effect of these agents contrasts sharply with CA-4's ineffectiveness when used alone or together with radiation, conventional antiangiogenics, biologics, or chemotherapy (19, 22–24, 42–45). SSRBCs' vaso-occlusive surge unleashed by CA-4-SR–induced tumor endothelial cell injury, therefore, appears to provide a therapeutic advantage over other combinations.

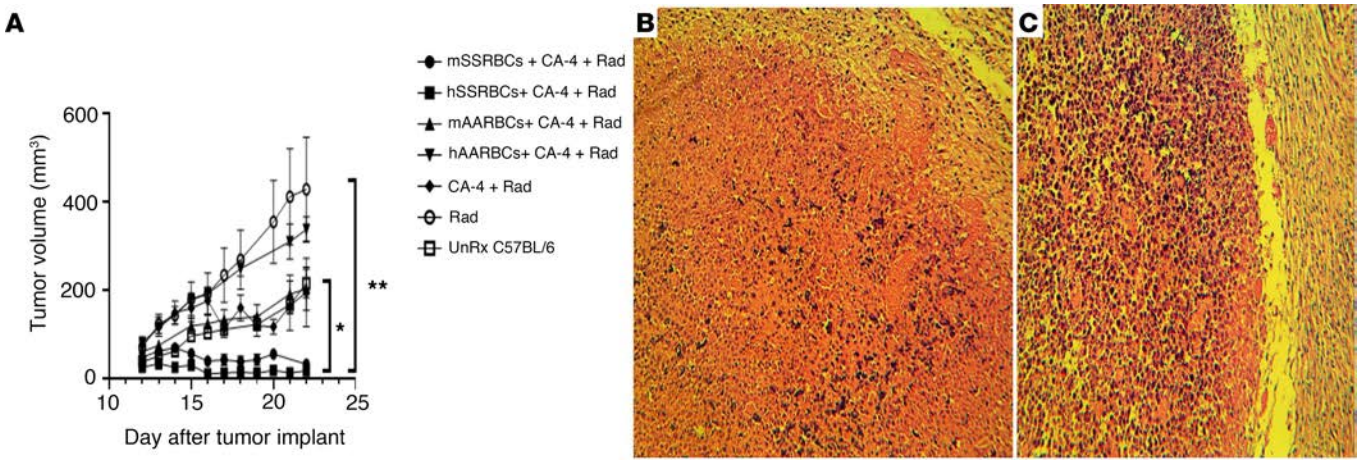

Figure 5. Regression of established LLC in C57BL/6J mice obtained on day 22 after treatment with tumor SR (10 Gy) on day 12 followed by CA-4 plus passive infusion of human or mouse SSRBCs (triple therapy) on days 13, 15, and 18. (**A**) Tumor regression with human or mouse SSRBC-based triple agent therapy exceeded that of human AARBC-based triple agent therapy (*P = 0.008), mouse AARBC-based triple therapy (*P = 0.009), and all other dual and single treatments (**$P \leq 0.009$, 2-tailed Student's t test; n = 6). (**B** and **C**) Histopathology of tumor sections obtained on day 22 from mice treated with SSRBC-based triple therapy shows extensive tumor vaso-occlusion and surrounding necrosis enveloping the tumor rim associated with mononuclear cell infiltration (original magnification, ×25).

SR's contribution to the tumor vaso-occlusive effect and infarction when combined with CA-4 and SSRBCs is likely due to cumulative tumor endothelial injury induced by SR's ability to activate endothelial ROS and produce mitotically based cell death (29–31). Tumor cells showing signs of radiation injury were engulfed in the tumoricidal infarction, suggesting that radiation-injured tumor cells may be more susceptible to SSRBC-mediated infarction akin to radiated cardiac tissue following experimental myocardial infarction induced by vascular ligation (46).

A surprising discovery is the ability of small amounts of passively infused human or mouse SSRBCs but not AARBCs to induce tumor killing in the tumor-bearing C57BL/6J mice treated with CA-4-SR. This finding indicates that this treatment is applicable to humans generally and not confined to tumors in subjects with sickle cell anemia. Using a microfluidic flow system, recent studies showed that as little as 10% SSRBCs in normal blood samples can significantly alter its viscosity and conductance (47, 48). This is ascribed to the presence of SSRBCs rendered rigid after multiple cycles of oxygenation-deoxygenation. Further studies to phenotype and characterize the conductance of the infused SSRBCs using this and similar integrative techniques will be useful in screening, selecting, and standardizing the SSRBC infusate for antitumor activity.

The accelerated growth of LLC noted in SSKI mice relative to AAKI mice has been previously noted in 4T1 tumors following SSRBC infusion (16). In the latter case, it may be ascribed to SSRBC-induced tumor vaso-occlusion resulting in increased tumor hypoxia and release of SSRBC-derived heme. Both heme and hypoxia activate HIF-1α and synthesis of VEGF and heme oxygenase, known stimulants of tumor angiogenesis and tumor growth (49). Previously, the addition of the competitive heme oxygenase inhibitor zinc protoporphyrin to SSRBCs abrogated the accelerated tumor growth (16), whereas in the present system, the rapidity and magnitude of the tumor cell and stromal eradication induced by SSRBC-based triple therapy likely aborted the synthesis of both heme oxygenase and hypoxia-inducible factors.

With respect to clinical translation and toxicity, SSRBC infusions in this and previous studies have been delivered safely to more than 100 tumor-bearing mice with no significant toxicity (15, 16). Because SSRBCs largely target hypoxic vasculature with upregulated adhesion receptors, patients with cancer who have vascular diseases bearing an underlying chronic oxidative stress signature such as hypertension and atherosclerotic cardio- and cerebrovascular disease (50) might be at higher risk of SSRBC treatment. The risk in these settings, however, may be no greater than that of many widely used cancer cytotoxics (e.g., doxorubicin), antiangiogenic agents (e.g., bevacizumab), and biologics (e.g., IL-2), which are known to exacerbate these vascular conditions. The assessment of prospective patients receiving SSRBC

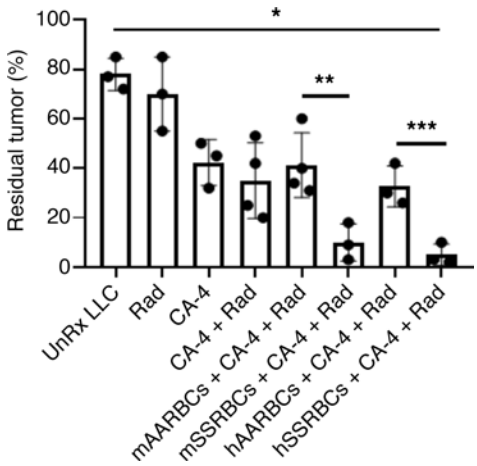

Figure 6. Residual viable LLC in sections from mice bearing established LLC obtained on day 22 after treatment with tumor SR (10 Gy) on day 12 followed by CA-4 plus passive infusion of human or mouse SSRBCs (triple therapy) on days 13, 15, and 18. Residual tumors in mice treated with mouse or human SSRBC-based triple agent therapy was significantly diminished relative to that of mice treated with mouse or human AARBC-based triple therapy (**P = 0.001 and ***P = 0.003, respectively). Residual tumors in mice treated with mouse or human SSRBC-based triple agent therapy were also significantly reduced relative to mice receiving dual or single treatments (*$P \leq 0.0001$, 2-tailed Student's t test; n = 3–4).

treatment would be similar to that of patients at risk of chemotherapy-associated venous thromboembolism. By excluding subjects showing an inflammatory and procoagulant phenotype and using small-volume SSRBC infusions, the risk of SSRBC treatment may be mitigated (51). Based on the efficacy with low-volume passive SSRBC infusions as described herein, we plan to use ABO-matched human SSRBCs differentiated from sickle stem/progenitor cells for transfusion into patients with advanced cancer along with parenteral vascular disrupting agent and sublethal tumor radiation.

Finally, we show that CA-4-SR–injured tumor microvessels license SSRBCs to unleash broadly propagated tumor vaso-occlusion that envelops treatment-resistant tumor niches and produces complete tumor regression. We term this response "induced vaso-occlusive lethality," wherein CA-4-SR is recast in the role of remodeling the microvascular environment for a massive surge of SSRBC-driven tumor infarction. When strategically deployed, these innovative tools constitute a major conceptual advance with compelling translational potential.

Methods

Mice. All animal procedures were approved by the UAB Institutional Animal Care and Use Committees or the Animal Use Committees in compliance with the Guide for the Care and Use of Laboratory Animals. Male and female mice 8 to 12 weeks of age weighing 19 to 26 grams were used. C57BL/6J, SSKI (B6; 129-Hba$^{tm1(HBA/Tow}$ Hbb$^{tm2(HBG1,HBB*/Tow}$/J), and AAKI (B6; 129-Hba$^{tm1(HBA/Tow}$ Hbb$^{tm3(HBG1,HBB)Tow}$/J) were obtained from a breeding colony maintained at the UAB animal research facility. Quantitative trait locus evaluation of SSKI and AAKI mice indicated that they are predominantly B6 and exhibit up to 30% of 129 genes. The animals were housed 7 animals per cage in a 12-hour light-dark cycle with food and water ad libitum.

Tumor cell lines and pharmaceuticals. The LLCs were obtained from ATCC. CA-4 was obtained from Sigma-Aldrich and pimonidazole hydrochloride [1-[(2-hydroxy-3-piperidinyl)propyl]-2-nitroimidazole–hydrochloride] from Hypoxyprobe Inc. Caki-1 cells were supplied by Dietmar Siemann (Department of Radiation Oncology, University of Florida, Gainesville, Florida, USA).

Hyperspectral imaging. In vivo hyperspectral imaging experiments with mouse window chamber tumors were conducted in accordance with a protocol approved by the University of Florida Institutional Animal Care and Use Committee. Hemoglobin saturation determinations in the tumor microvasculature using hyperspectral imaging information was described previously (52). A Zeiss Axioskop 2 microscope (Carl Zeiss, Inc.) served as the imaging platform. Images were acquired with a CCD camera (DVC Company), and bandlimited optical filtering for hyperspectral imaging was accomplished with a C-mounted liquid crystal tunable filter (CRI Inc.). Image processing was performed using Matlab software (MathWorks). Microvessel-based pixel counts of vessels in window chamber tumors were quantified as a fraction of microvessel pixels over the total number of micropixels in the tumor as described (52).

Collection, preparation, and treatment of human and mouse RBCs. Normal RBCs were obtained from normal healthy adults and SSRBCs from patients with homozygous sickle cell anemia. Fresh blood samples were collected into citrate tubes. RBCs were separated from the buffy coat by gravity at 4°C for at least 2

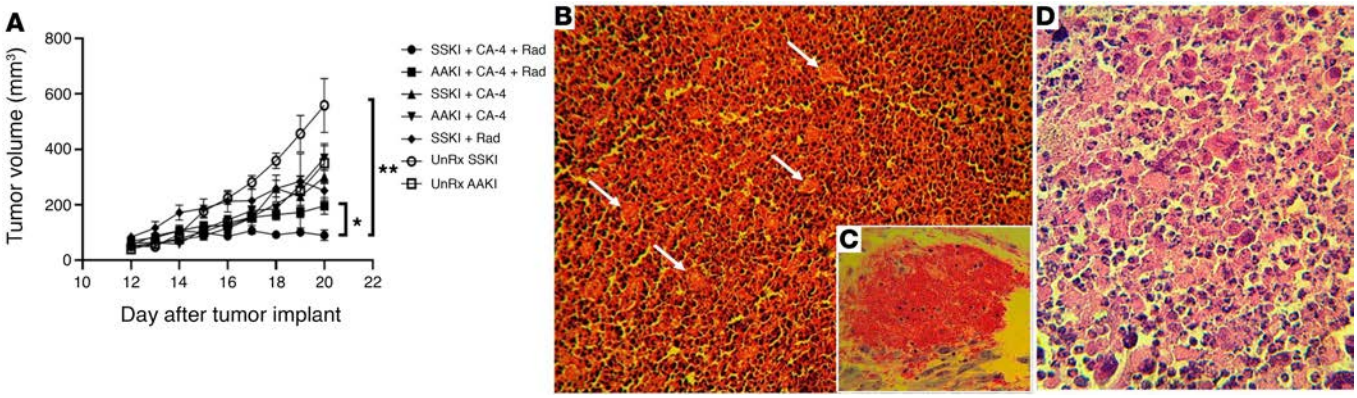

Figure 7. Regression of established LLC in SSKI or AAKI mice obtained on day 20 after treatment with tumor SR (10 Gy) on day 12 followed by CA-4 on days 13, 15, and 18. (**A**) Tumor regression in SSKI mice exceeded that of similar therapy in AAKI mice (*P = 0.01) and all other dual and single treatments (**$P \leq 0.008$, 2-tailed Student's t test; $n = 6$). (**B**) Histopathology of tumor sections obtained from SSKI mice at day 20 after treatment with SR (10 Gy) on day 12 followed by CA-4 on days 13, 15, and 18 shows extensive tumor vaso-occlusion (arrows) and infarction enveloping the core and tumor periphery (original magnification, ×25). (**C**) Representative tumor blood vessel occluded with tightly packed sickle cells (original magnification, ×40). (**D**) Tumor cell necrosis, mononuclear cell infiltrate adjacent to occluded blood vessels is shown (original magnification, ×40).

hours. Plasma and buffy coat were removed by aspiration and RBCs were washed 4 times in sterile PBS with 1.26 mM Ca^{2+}, 0.9 mM Mg^{2+} (pH 7.4). SSRBCs or AARBCs were obtained from SSKI or AAKI mice by cardiac puncture into EDTA-coated tubes. RBCs were separated and washed as described previously (16). The cells were diluted to Hct 50% in PBS and administered intravenously via the retro-orbital vein.

Radiation. Radiation was carried out using an X-RAD 320 irradiator (Precision X-Ray). Mice were anesthetized with 1.6% Avertin in PBS (Sigma-Aldrich T48402-5G) and positioned in a metal jig exposing the tumor while shielding the body. In all studies using radiation, it was delivered to tumor as a single dose of 10 Gy at 1 Gy/minute.

Tumor therapy studies. Mice were injected in the right flank with 10^5 LLC cells in volume of 50 μl containing 25 μl of Matrigel (Thermo Fisher Scientific). Tumor volumes were measured daily with standard calipers, and volumes were calculated as length × width^2/2, in which length is the long axis and width is the short axis. The endpoint was a tumor volume of 750 to 1500 mm^3. Lyophilized CA-4 was hydrated in sterile distilled water under dark conditions. In vivo studies were started when tumors reached a median diameter of 78 mm^3 (53–94 mm^3). In the passive transfer protocol, tumors were radiated with 10 Gy on day 12. On day 13, CA-4 30 mg/kg in 50 μl of sterile distilled water was administered intraperitoneally followed by intravenous delivery of human or mouse SSRBCs or AARBCs from SSKI mice or AAKI mice, respectively in 200 μl of PBS, Hct 50%. CA-4 and SSRBCs or AARBC treatment was repeated on days 15 and 18. Tumors were measured daily with Vernier calipers. Mice were euthanized if toxicity was evident or tumor burden exceeded 500 mm^3. In the SSKI treatment protocol, tumors established in SSKI or AAKI mice were radiated with 10 Gy on day 12 as described previously and treated with CA-4 30 mg/kg intraperitoneally on days 13, 15, and 18. Histologic and immunohistochemical samples were obtained on day 22 in the passive transfer study and on day 20 in the SSKI protocol.

Pimonidazole uptake in tumors. Pimonidazole at doses of 60 mg/kg body weight in 1 ml 0.9% normal saline was administered intravenously to the tumor-bearing mice. Tumors were harvested 60 minutes after Hypoxyprobe-1 administration. The tumors were dissected and fixed in phosphate-buffered 4% paraformaldehyde and embedded in paraffin casts before 5-μm histological sections were cut.

Histology and immunohistochemistry. Mice were anesthetized with ketamine and tumors were excised surgically. The tumors were fixed with formalin and embedded in paraffin. Serial sections 5 μm thick were cut from the formalin-fixed, paraffin-embedded tissue blocks and floated onto charged glass slides (Super-Frost Plus, Thermo Fisher Scientific) and dried overnight at 60°C. Sections were stained with hematoxylin and eosin (H&E). For immunohistochemical staining, tumor sections were deparaffinized and hydrated using graded concentration ratios of ethanol to deionized water. The sections were then incubated with 0.01 M Tris–1 mM EDTA buffer (pH 9) in a pressure cooker for 5 minutes. Sections were then washed in deionized water and transferred to 0.05 M Tris-based solution in 0.15 M NaCl with 0.1% v/v Triton X-100, pH 7.6 (TBST).

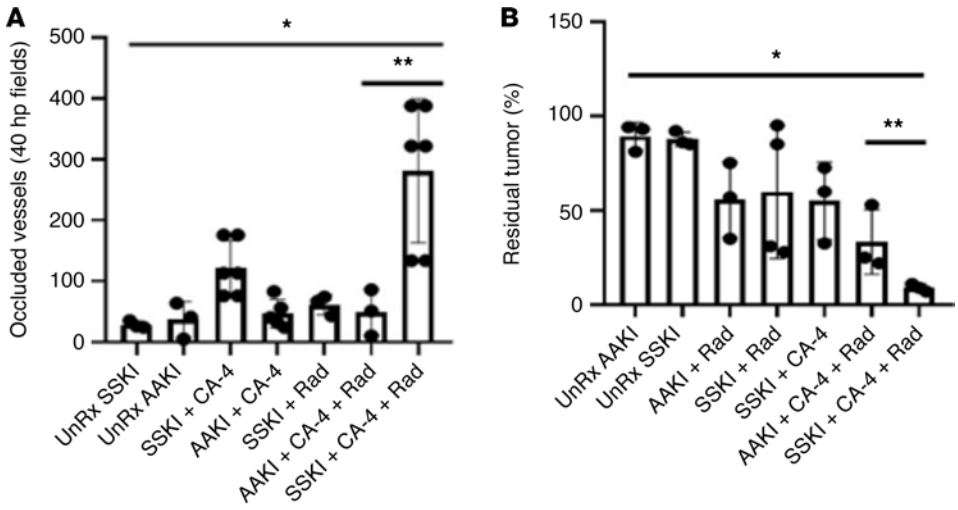

Figure 8. Quantification of vaso-occlusion and residual viable tumor in sections of established LLC obtained on day 20 from in SSKI and AAKI mice after treatment with tumor SR (10 Gy) on day 12 followed by CA-4 on days 13, 15, and 18. (**A**) Vessel closure in SSKI mice treated with radiation and CA-4 exceeded that of similarly treated AAKI mice (**P = 0.003) and all other controls (*$P \leq 0.003$, n = 4–6). (**B**) Residual viable LLC in sections obtained on day 20 from SSKI mice treated with sublethal radiation (10 Gy) on day 12 followed by CA-4 on days 12, 15, and 18 was significantly diminished relative to similarly treated AAKI mice (**P = 0.005) and all other controls (*$P < 0.01$, 2-tailed Student's t test; n = 3).

Endogenous peroxidase was blocked with 3% hydrogen peroxide for 10 minutes. To reduce further nonspecific background staining, slides were incubated with 3% normal goat serum (Sigma-Aldrich) for 30 minutes at room temperature. Slides then were incubated overnight at 4°C with rabbit anti–mouse Ki-67 monoclonal antibody at 1:50 dilution (Thermo Fisher Scientific, RM-9106-S0) or mouse anti-pimonidazole IgG1 monoclonal antibody at 1:50 dilution (Hypoxyprobe). Negative controls were produced by eliminating the primary antibodies from the diluents. After washing with TBST, sections treated with anti–Ki-67 or anti-pimidazole were incubated with 1:1000 dilution of goat anti-rabbit IgG H&L (HRP) (Abcam, ab6721) or 1:100 dilution of goat anti-mouse IgG H&L (HRP) (Abcam, ab6789), respectively. Diaminobenzidine (DAB; Scy Tek Laboratories) was used as the chromagen and hematoxylin (no. 7211, Richard-Allen Scientific) as the counterstain.

Histochemical quantification of residual viable tumor, fraction of hypoxic cells, tumor vaso-occlusion, and Ki-67–positive cells. Histochemical quantification of Ki-67–immunopositive cells was carried out at ×40 original magnification on 30 separate fields of tumor and examined using a Leitz Diaplan microscope. The total number of Ki-67–immunopositive cells was determined. The area showing pimidazole staining was determined by using ImageJ software (NIH). The analyses were performed using original magnification of ×10. Values of the fractional area of pimidazole positivity were computed as a function of the total tumor area. Fraction of immunohistochemically hypoxic cells (IHFs) was calculated as: $IHF = AF_{pim}/A_{total}$ in which AF_{pim} is the fraction showing pimonidazole staining and A_{total} is the total tumor area. Quantification of vaso-occlusion in tumors was carried out by enumerating the total number of occluded microvessels in 40 fields of H&E-stained tumor sections at ×40 original magnification. Microvessels were occluded when at least 80% of the vessel lumen was filled with erythrocytes. Residual viable tumor area was determined on slides of sections from 3 to 4 treated tumors stained within each group. The H&E–stained slides were scanned at 1200 dpi and photographed as a TIFF image. The necrotic and viable areas of these sections were identified histologically and corroborated using ImageJ software. Residual viable tumor area was expressed as the percentage of pixels in the total area minus the area of the necrotic regions in the entire tumor section (53, 54). Statistical analysis was based on a mean of 3 to 4 tumors per group.

Statistics. For comparison of individual data points, 2-tailed Student's t test was applied to determine statistical significance along with ANOVA 1-way analysis of variance with Bonferroni's adjustment. $P \leq 0.05$ values were considered statistically significant and $P < 0.01$ values were considered highly statistically significant.

Study approval. The present studies in animals and/or humans were reviewed and approved by institutional review boards at the University of Alabama Medical School at Birmingham, Alabama, and University of Florida Medical School at Gainesville, Florida. Subjects provided informed consent prior to their participation in the study.

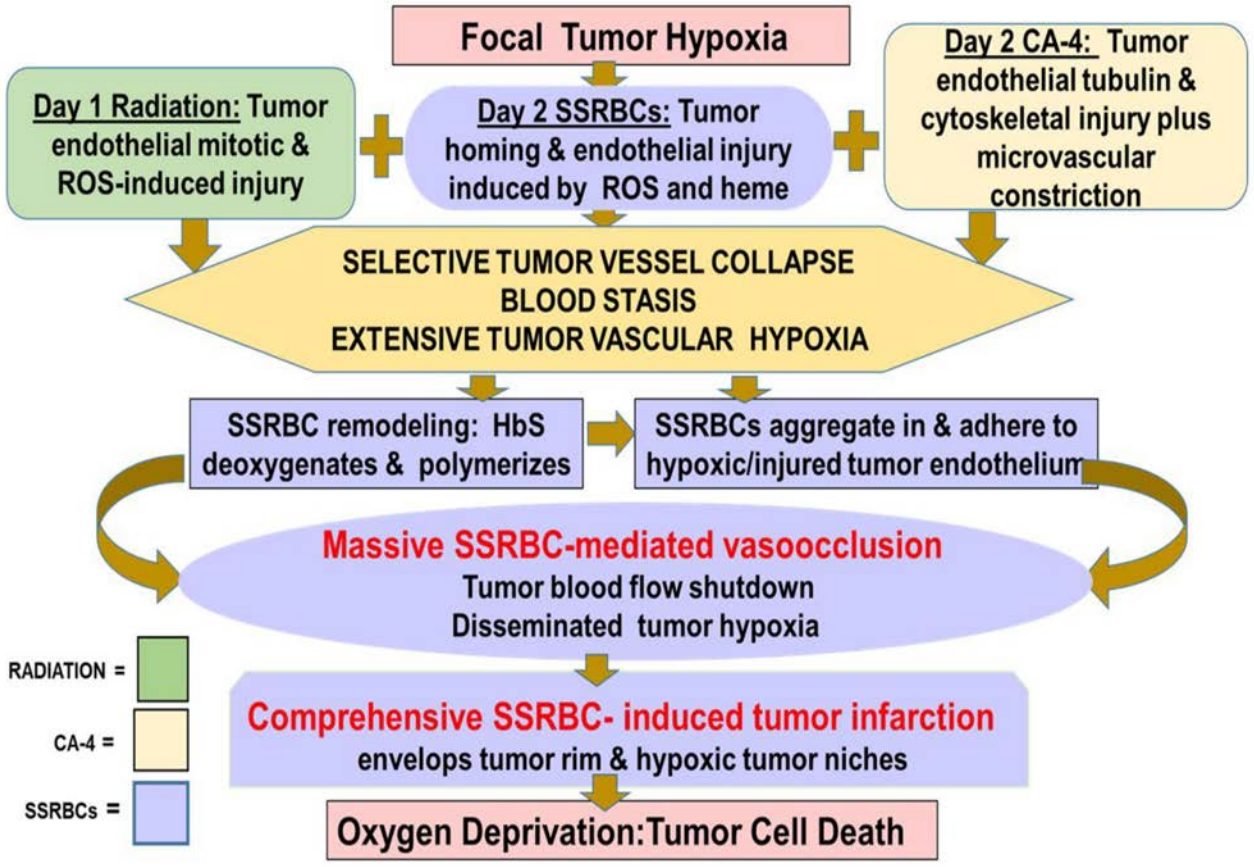

Figure 9. Chain of events leading to massive SSRBC-mediated tumor vaso-occlusion and infarction in tumor microvessels conditioned for tumor vascular injury by CA-4 and tumor SR is shown. Untreated LLC shows a modest degree of focal tumor hypoxia. Introduction of sublethal radiation initiates tumor endothelial mitotic-based and oxidant-mediated injury followed within 24 hours by CA-4, which induces endothelial tubulin depolymerization and cytoskeletal injury. Subsequent addition of SSRBCs and their contact with the tumor endothelium induces further oxidant-mediated damage. The combined effect results in severe tumor hypoxia and vascular injury resulting in blood flow stagnation. Under these conditions, HbS deoxygenates and polymerizes, and the SSRBCs assume the sickle morphology forming aggregates that adhere to the tumor vessel wall. A surge of SSRBC-mediated tumor vaso-occlusion ensues with disseminated mononuclear cell infiltration and infarction. The scale of the tumor infarction engulfs the entire tumor including treatment-resistant hypoxic niches and the tumor rim. The comprehensive tumor eradication leads to tumor regression and a major histopathological treatment effect.

Author contributions

DST conceived and designed the study. TMT, CWS, LCW, MW, BSS, and DST analyzed the data and edited the manuscript. CWS, LCW, DW, JT, LW, MW, BSS, and DST conducted the experiments. DST wrote the manuscript.

Acknowledgments

This work was supported by NIH grant R01HL057619 and the Azore (NP) Foundation. DST is recipient of the Doctors Cancer Research Foundation Prize. The funders had no role in study design, data collection and analysis, decision to publish, or preparation of the manuscript.

Address correspondence to: David S. Terman, Department of Biochemistry and Molecular Genetics, University of Alabama School of Medicine at Birmingham, Birmingham, Alabama 35294, USA. Phone: 831.624.8569; Email: dst@sbcglobal.net.

1. Wilson WR, Hay MP. Targeting hypoxia in cancer therapy. *Nat Rev Cancer*. 2011;11(6):393–410.
2. Harris AL. Hypoxia-a key regulator factor in tumor growth. *Nat Rev Cancer*. 2002; 2(1):38–47.
3. Kim JJ, Tannock IF. Repopulation of cancer cells during therapy: an important cause of treatment failure. *Nat Rev Cancer*. 2005;5(7):516–525.
4. Kerbel RS. Tumor angiogenesis. *N Engl J Med*. 2008;358(19):2039–2049.

5. Pries AR, Hopfner M, Noble F, Dewhirst MW, Secomb TW. The shunt problem: control of functional shunting in normal and tumour vasculature. *Nat Rev Cancer.* 2010;10(8):587–593.
6. Brunelle JK, Chandel NS. Oxygen deprivation induced cell death: an update. *Apoptosis.* 2002;7(6):475–82.
7. Abdollahi A, Folkman J. Evading tumor evasion: current concepts and perspectives of anti-angiogenic cancer therapy. *Drug Resist Updat*. 2010;13(1–2):16–28.
8. Bergers G, Hanahan D. Modes of resistance to anti-angiogenic therapy. *Nat Rev Cancer*. 2008;8(8):592–603.
9. Ma S, Pradeep S, Hu W, Zhang D, Coleman R, Sood A. The role of tumor microenvironment in resistance to anti-angiogenic therapy. *F1000Res*. 2018;15;7:326.
10. Vasuri F, et al. Revisiting the role of pathological analysis in transarterial chemoembolization-treated hepatocellular carcinoma after transplantation. *World J Gastroenterol*. 2014;20(37):13538–13545.
11. Tannock IF, Lee CM, Tunggal JK, Cowan DSM, Egorin MJ. Limited penetration of anticancer drugs through tumor tissue: a potential cause of resistance of solid tumors to chemotherapy. *Clin Cancer Res*. 2002;8(3):878–884.
12. Manwani D, Frenette PS. Vaso-occlusion in sickle cell disease: pathophysiology and novel targeted therapies. *Blood*. 2013;122(24):3892–3898.
13. Rees DC, Williams TN, Gladwin MT. Sickle-cell disease. *Lancet*. 2010;376(9757):2018–2031.
14. Ballas SK, Mohandas N. Sickle red cell microrheology and sickle blood rheology. *Microcirculation*. 2004;11(2):209–225.
15. Sun CW, Willmon C, Wu LC, Townes TM, Terman DS. Sickle cells abolish melanoma tumorigenesis in hemoglobin S knockin mice and augment the tumoricidal effect of oncolytic virus in vivo. *Front Oncol*. 2016;6:166.
16. Terman DS, et al. Sickle erythrocytes target cytotoxics to hypoxic tumor microvessels potentiate a tumoricidal response. *PLoS One*. 2013;8(1):e52543.
17. Siemann DW, Shi W. Dual targeting of tumor vasculature: combining avastin and vascular disrupting agents (CA4P or OXi4503). *Anticancer Res*. 2008;28(4B): 2027–2031.
18. Tozer GM, et al. Mechanisms associated with tumor vascular shut-down induced by combretastatin A-4 phosphate: intravital microscopy and measurement of vascular permeability. *Cancer Res*. 2001; 61(17):6413–6422.
19. Tozer GM, Kanthou C, Baguley BC. Disrupting tumour blood vessels. *Nat Rev Cancer*. 2005;5(6):423–435.
20. Hill SA, Tozer GM, Pettit GR, Chaplin DJ. Preclinical evaluation of the antitumour activity of the novel vascular targeting agent Oxi 4503. *Anticancer Res*. 2002;22(3):1453–1458.
21. Siemann DW. The unique characteristics of tumor vasculature and preclinical evidence for its selective disruption by tumor-vascular disrupting agents. *Cancer Treatment Rev.* 2011;37(1):63–74.
22. Salmon HW, Siemann DW. Effect of the second-generation vascular disrupting agent OXi4503 on tumor vascularity. *Clin Cancer Res*. 2006;12(13):4090–4094.
23. Clémenson C, Chargari C, Deutsch E. Combination of vascular disrupting agents and ionizing radiation. *Crit Rev Oncol Hematol*. 2013;86(2):143–160.
24. von Pawel J, et al. DISRUPT: a randomised phase 2 trial of ombrabulin (AVE8062) plus a taxane-platinum regimen as first-line therapy for metastatic non-small cell lung cancer. *Lung Cancer*. 2014;85(2):224–229.
25. Lee JA, Biel NM, Kozikowski RT, Siemann DW, Sorg BS. In vivo spectral and fluorescence microscopy comparison of microvascular function after treatment with OXi4503, Sunitinib and their combination in Caki-2 tumors. *Biomed Opt Express*. 2014;5(6):1965–1979.
26. Wankhede M, Dedeugd C, Siemann DW, Sorg BS. In vivo functional differences in microvascular response of 4T1 and Caki-1 tumors after treatment with OXi4503. *Oncol Rep*. 2010;23(3):685–692.
27. Noguchi CT, Torchia DA, Schechter AN. Determination of deoxyhemoglobin S polymer in sickle erythrocytes upon deoxygenation. *Proc Natl Acad Sci U S A*. 1980;77(9):5487–5491.
28. Rofstad EK, Måseide K. Radiobiological and immunohistochemical assessment of hypoxia in human melanoma xenografts: acute and chronic hypoxia in individual tumours. *Int J Radiat Biol*. 1999;75(11):1377–1393.
29. Connell PP, Hellman S. Advances in radiotherapy and implications for the next century: a historical perspective. *Cancer Res*. 2009;69(2):383–392.
30. Garcia-Barros M, et al. Tumor response to radiotherapy regulated by endothelial cell. apoptosis. *Science.* 2003;300(5622):1155–1159.
31. Paris F, et al. Endothelial apoptosis as the primary lesion initiating intestinal radiation damage in mice. *Science*. 2001;293(5528):293–297.
32. Prise VE, Honess DJ, Stratford MR, Wilson J, Tozer GM. The vascular response of tumor and normal tissues in the rat to the vascular targeting agent, combretastatin A-4-phosphate, at clinically relevant doses. *Int J Oncol*. 2002;21(4):717–726.
33. Hellmann MD, et al. Pathological response after neoadjuvant chemotherapy in resectable non-small-cell lung cancers: proposal for the use of major pathological response as a surrogate endpoint. *Lancet Oncol*. 2014;15(1):e42–e50.
34. Pataer A, et al. Histopathologic response criteria predict survival of patients with resected lung cancer after neoadjuvant chemotherapy. *J Thorac Oncol*. 2012;7(5):825–832.
35. Kanthou C, Tozer GM. The tumor vascular targeting agent combretastatin A-4 phosphate induces reorganization of the actin cytoskeleton and early membrane blebbing in human endothelial cells. *Blood*. 2002; 99(6):2060–2069.
36. Vincent L, et al. Combretastatin A4 phosphate induces rapid regression of tumor neovessels and growth through interference with vascular endothelial-cadherin signaling. *J Clin Invest*. 2005;115(11):2992–3006.
37. Hori K, Saito S. Microvascular mechanisms by which the combretastatin A-4 derivative AC7700 (AVE8062) induces tumour blood flow stasis. *Br J Cancer.* 2003;89(7):1334–1344.
38. Kaul DK, Liu X, Zhang X, Ma L, Hsia C, Nagel RL. Inhibition of sickle red cell adhesion and vasoocclusion in the microcirculation by antioxidants. *Am J Physiol Heart Circ Physiol.* 2006;291(1):H167–H175.
39. Balla G, Vercellotti BM, Muller-Eberhard U, Eaton J, Jacob HS. Exposure of endothelial cells to free heme potentiates damage mediated by granulocytes toxic oxygen species. *Lab Invest*. 1991;64(5):648–655.
40. Belcher JD, et al. Heme triggers TLR4 signaling leading to endothelial cell activation and vaso-occlusion in murine sickle cell disease. *Blood*. 2014;123(3):377–390.
41. Rammohan A, et al. Embolization of liver tumors: past, present and future. *World J Radiol*. 2012;4(9):405–412.

42. Nathan P, et al. Phase I trial of combretastatin A4 phosphate (CA4P) in combination with bevacizumab in patients with advanced cancer. *Clin Cancer Res*. 2012;18(12):3428–3439.
43. Garon EB, Neidhart JD, Gabrail NY, de Oliveira MR, Balkissoon J, Kabbinavar F. A randomized Phase II trial of the tumor vascular disrupting agent CA4P (fosbretabulin tromethamine) with carboplatin, paclitaxel, and bevacizumab in advanced non-squamous non-small-cell lung cancer. *Onco Targets Ther*. 2016;9:7275–7283.
44. Rustin GJ, et al. A Phase Ib trial of CA4P (combretastatin A-4 phosphate), carboplatin, and paclitaxel in patients with advanced cancer. *Br J Cancer*. 2010;102(9):1355–1360.
45. Stevenson JP, et al. Phase I trial of the antivascular agent combretastatin A4 phosphate on a 5-day schedule to patients with cancer: magnetic resonance imaging evidence for altered tumor blood flow. *J Clin Oncol*. 2003;21(23):4428–4438.
46. Luo L, et al. Ionizing radiation impairs endogenous regeneration of infarcted heart: an in vivo ^{18}F-FDG PET/CT and ^{99m}Tc-tetrofosmin SPECT/CT study in mice. *Radiat Res*. 2017;187(1):89–97.
47. Lu X, Wood DK, Higgins JM. Deoxygenation reduces sickle cell blood flow at arterial oxygen tension. *Biophys J*. 2016;110(12):2751–2758.
48. Wood DK, Soriano A, Mahadevan L, Higgins JM, Bhatia SN. A biophysical indicator of vaso-occlusive risk in sickle cell disease. *Sci Transl Med*. 2012; 4(123):123–126.
49. Lee PJ, et al. Hypoxia-inducible factor-1 mediates transcriptional activation of the heme oxygenase-1 gene in response to hypoxia. *J Biol Chem*. 1997;272(9):5375–5381.
50. Madamanchi NR, Vendrov A, Runge MS. Oxidative stress and vascular disease. *Arterioscler Thromb Vasc Biol*. 2005;25(1):29–38.
51. Khorana AA, et al. Venous thromboembolism prophylaxis and treatment in cancer: a consensus statement of major guidelines panels and call to action. *J Clin Oncol*. 2009; 27(29):4919–4926.
52. Sorg BS, Moeller BJ, Donovan O, Cao Y, Dewhirst MW. Hyperspectral imaging of hemoglobin saturation in tumor microvasculature and tumor hypoxia development. *J Biomed Opt*. 2005;10(4):44004.
53. Jun J, et al. Effect of intermittent hypoxia on atherosclerosis in apolipoprotein E-deficient mice. *Atherosclerosis*. 2010;209(2):381–386.
54. Kojima Y, et al. CD47-blocking antibodies restore phagocytosis and prevent atherosclerosis. *Nature*. 2016; 536(7614):86–90.